AD-A139 298 PHOTOACOUSTIC IMAGING(U) STANFORD UNIV CA EDWARD L GINZTON LAB OF PHYSICS C F QUATE DEC 83 GL-3672 AFOSR-TR-84-0156 AFOSR-82-0248 1/1

UNCLASSIFIED F/G 20/6 NL

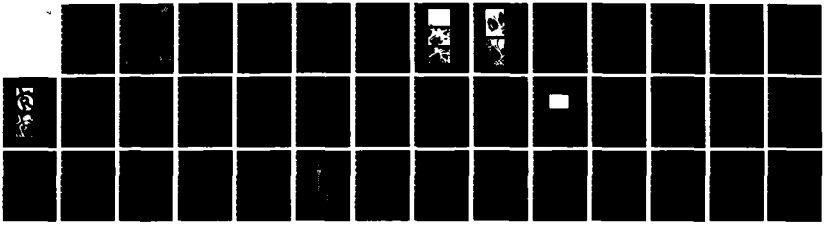

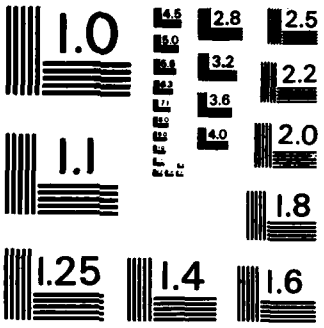

Edward L. Ginzton Laboratory
W. W. Hansen Laboratoires of Physics
Stanford University
Stanford, CA 94305

PHOTOACOUSTIC IMAGING

Annual Report

for the period

June 30, 1982 - June 29, 1983

Sponsored by

Air Force Office of Scientific Research (AFSC)

AFOSR/NE under Grant No. AFOSR-82-0248

Principal Investigator:

C. F. Quate

G.L. Report No. 3672

December 1983

UNCLASSIFIED

SECURITY CLASSIFICATION OF THIS PAGE (When Data Entered)

REPORT DOCUMENTATION PAGE		READ INSTRUCTIONS BEFORE COMPLETING FORM
1. REPORT NUMBER AFOSR-TR- 84-0156	2. GOVT ACCESSION NO.	3. RECIPIENT'S CATALOG NUMBER
4. TITLE (and Subtitle) PHOTOACOUSTIC IMAGING		5. TYPE OF REPORT & PERIOD COVERED Annual Report June 30 82 - June 29 83
		6. PERFORMING ORG. REPORT NUMBER G.L.-Report No. 3672
7. AUTHOR(s) C. F. Quate Clayton Williams		8. CONTRACT OR GRANT NUMBER(s) AFOSR-82-0248
9. PERFORMING ORGANIZATION NAME AND ADDRESS Edward L. Ginzton Laboratory Stanford University Stanford, California 94305		10. PROGRAM ELEMENT, PROJECT, TASK AREA & WORK UNIT NUMBERS 2306/A2 61102F
11. CONTROLLING OFFICE NAME AND ADDRESS AFOSR/NE Building 410 Bolling AFB, D.C. 20332		12. REPORT DATE December 1983 13. NUMBER OF PAGES 40
14. MONITORING AGENCY NAME & ADDRESS(if different from Controlling Office)		15. SECURITY CLASS. (of this report) UNCLASSIFIED 15a. DECLASSIFICATION/DOWNGRADING SCHEDULE

16. DISTRIBUTION STATEMENT (of this Report)

"Approved for public release; distribution unlimited"

17. DISTRIBUTION STATEMENT (of the abstract entered in Block 20, if different from Report)

18. SUPPLEMENTARY NOTES

19. KEY WORDS (Continue on reverse side if necessary and identify by block number)

Photoacoustics	Photothermal Imaging	Photoacoustic Imaging
Thermal Waves	Recrystallized Silicon	Acoustic Microscope

20. ABSTRACT (Continue on reverse side if necessary and identify by block number)

This report includes a description of two new high frequency photoacoustic and photothermal imaging systems developed in the reporting period. Also included is a photoacoustic study of laser recrystallized silicon, and an extension to three dimensions of the theory of thermo-acoustic generation in solids.

DD FORM 1 JAN 73 1473 EDITION OF 1 NOV 65 IS OBSOLETE

UNCLASSIFIED

SECURITY CLASSIFICATION OF THIS PAGE (When Data Entered)

TABLE OF CONTENTS

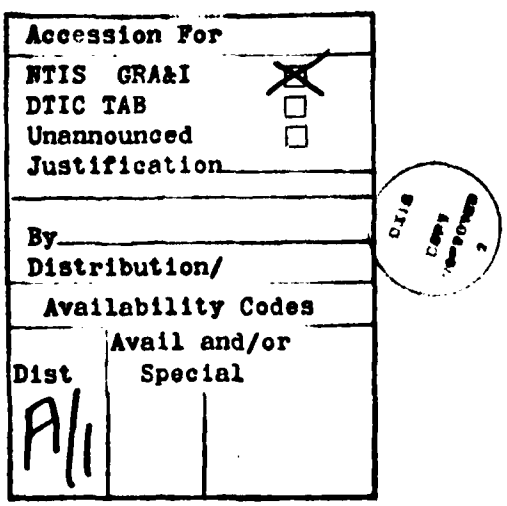

SECTION 1

HIGH RESOLUTION PHOTOACOUSTIC IMAGING

This report will summarize the research done in the area of photoacoustic imaging for the period July 1982 to July 1983. The progress that has resulted from the support that was furnished under this program has brought about several new developments and contributions to the field of photoacoustic imaging. These contributions will be briefly overviewed in this introduction, and further detail will be given in the following sections.

At the time for the proposal of this research, we had just obtained high resolution photoacoustic images of laser recrystalized silicon films on insulating substrates. Section 2 will summarize the complete study done in this area. The results indicate that the source of the dramatic contrast in the images is the variation in the adhesion properties of the different recrystalized grains.

In Section 3, a new technique is described which has made possible the photoacoustic imaging of opaque materials. Until recently, this was not possible due to the fact that the optical power used as the heat source had to be focused through the substrate to allow collection of the acoustic power generated at the front surface. Using liquid gallium as an acoustic coupler, it is now possible to collect the generated acoustic power as propagated through the substrate. This allows illumination of the surface to be imaged by the heating laser. Thus, optically opaque materials can now be investigated.

We have seen no three dimensional theory for photoacoustic generation in solids published to account for the highly focused optical sources that are used in high resolution photothermal imaging. When the thermal source is small compared to an acoustic wavelength, one dimensional theories are inadequate. We have, therefore, done some three dimensional theory for a modulated point source of heat. The three

SECTION 2

STUDY OF LASER RECRYSTALLIZED SILICON FILMS

In this section, we report the results of the study of laser recrystallized thin film silicon on quartz substrates. Laser recrystallization is currently an active area of research. Much effort has been made to grow large grain polysilicon with grain sizes of 100 microns from fine grain polysilicon using laser recrystallization. The recrystallization process is inherently traumatic, producing large changes in temperature in short times, inducing stresses and changes of mechanical structure. We expected that photoacoustics might be a sensitive probe to measure some of the parameters of the films after recrystallization. We looked at some recrystallized films and found that the photoacoustic response from grain to grain was very different, even when the grains had a common boundary. The variation in received power was measured to be as large as 8 db from grain to grain. This variation is not seen optically and only marginally in acoustic imaging. Figure 1 has a comparison of optical, acoustical, and photoacoustical images.

In all three images, the large thermal cracks are very apparent. The subgrain boundaries, however, are apparent only in the optical image, which is of higher resolution. There is no contrast from grain center to grain center in either the optical or acoustic images, whereas in the photoacoustic image it is clear that one grain is very much darker than the surrounding grains. See Figure 2. Note that the boundaries between the dark and light regions are very sharp.

To understand the variation of photoacoustic response from grain to grain, we used a one-dimensional model to calculate the generated acoustic power for silicon on quartz, and varied all of the characteristic material parameters of the silicon to identify which might be the source of the large variation of the photoacoustic response. Our numerical calculations indicated that no reasonable variation in

OPTICAL

PHOTOACOUSTIC

ACOUSTIC

LASER RECRYSTALIZED SILICON (0.5μm) ON QUARTZ SUBSTRATE

FIGURE 1

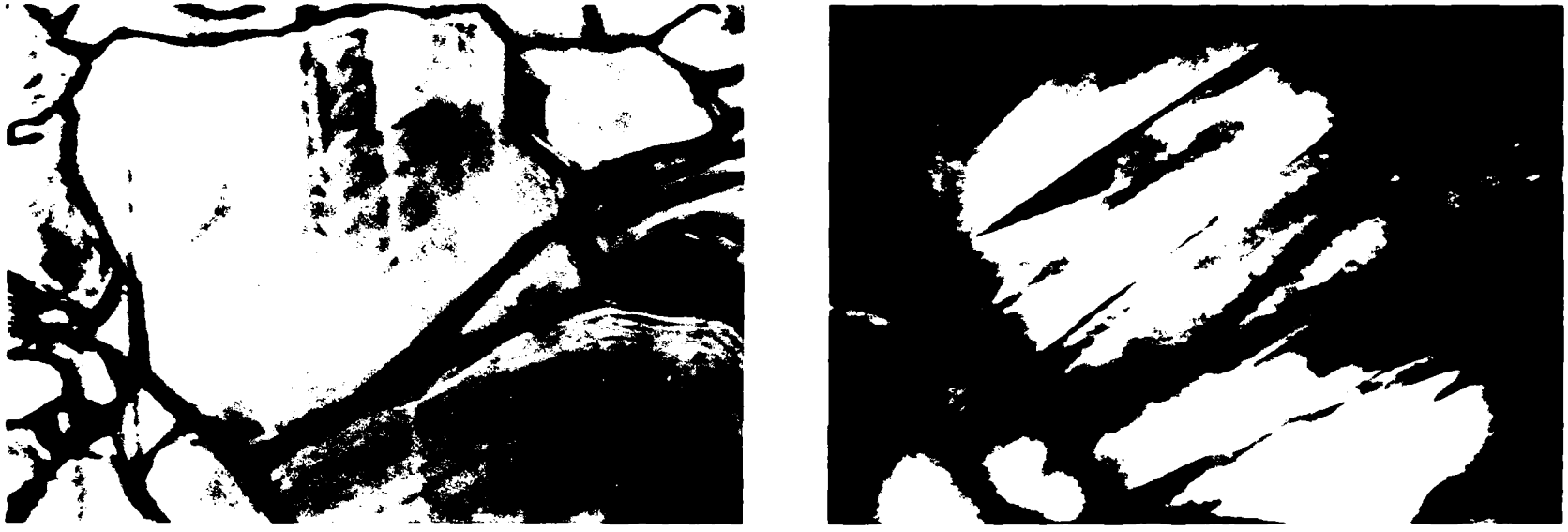

FIELD SIZE 300 μm

ACOUSTIC REFLECTION (1GHz)

PHOTOACOUSTIC (1GHz)

RECRYSTALIZED SILICON FILM (0.5μm) ON QUARTZ SUBSTRATE

FIGURE 2

the material constants of the silicon could explain this kind of contrast. We then considered adhesion as a possible source of contrast. We calculated the change in the far field generated acoustic power for the well adhered case and compared it with the unadhered case and found the difference to be approximately 6 db. This was very close to the measured value of 8 db. We also noticed in these images that near the thermal cracks, there was a darkening in the photo- acoustic images, indicating that the adhesion was poor in these regions also. We concluded that we were seeing the effects of non- uniform adhesion in these films. The contrast in acoustic reflection images of these laser recrystalized silicon films, though smaller, also supported this conclusion. The samples that we have looked at were provided by the research group of J.F. Gibbons of Stanford University. Until the photoacoustic images had revealed the inhomogeneities that existed in their recrystalized films, they were unaware of their presence.

This photoacoustic technique is a particularly good technique for looking at thin films. This is true because the film itself is the only source of photoacoustic power and, therefore, competes with no background. By contrast, in acoustic reflection imaging, the thin film only perturbs the impedance and surface wave velocity of the substrate. Therefore, the signal from the film must compete with the large signal which comes from the substrate. The sensitivity of the photoacoustic technique has allowed us to clearly identify inhomogeneities in laser recrystalized thin films that have not been identified by other techniques.

SECTION 3

PHOTOACOUSTIC IMAGING OF A FREE SURFACE

We report on a new acoustic coupling scheme that has been developed for the collection of thermally generated acoustics. This new scheme has several advantages over the previous method. In the photoacoustic imaging system that we have previously used, the optical power must be focused through a transparent substrate to the surface to be imaged. See the upper half of Figure 3.

The generated acoustic power is then coupled to the acoustic collection lens via a liquid (generally water). Although for many types of samples this scheme is adequate, the system has two limitations which restrict the class of materials that can be imaged. The first limitation is that the substrate must be optically transparent. This excludes many interesting materials and systems, one of which is silicon. When using visible wavelengths, the attenuation in the silicon does not allow the optical power to reach the surface to be imaged. The second limitation is that it is necessary to directly contact the surface to be imaged with the coupling liquid. Materials which are modified by or react with the coupling liquid cannot, therefore, be imaged using this technique.

We have now circumvented these limitations with a new coupling scheme. With the use of a larger acoustic lens, and gallium as a coupling liquid, it is now possible to couple the generated acoustic power through the sample substrate to the acoustic lens. This has allowed us to focus the optical power directly on to the surface to be imaged, thus providing a non-contacting technique for photoacoustic imaging, as well as eliminating the requirement of an optically transparent substrate. This second scheme is illustrated in the lower half of Figure 3. The upper figure shows the system in which the acoustic energy is coupled directly from the generating surface to the lens. The lower figure represents the system where the acoustic energy is

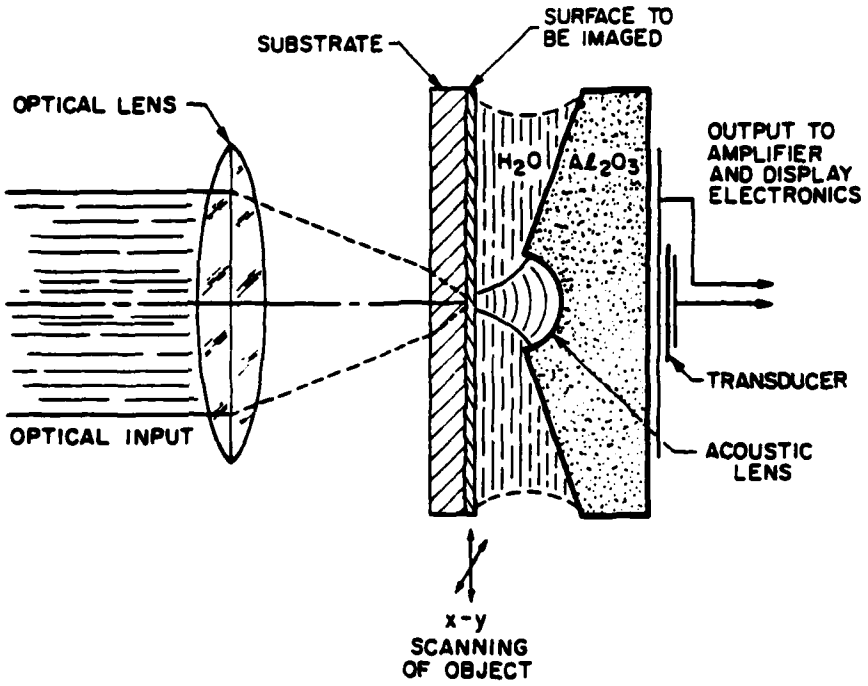

PHOTOACOUSTIC IMAGING OF A LOADED SURFACE

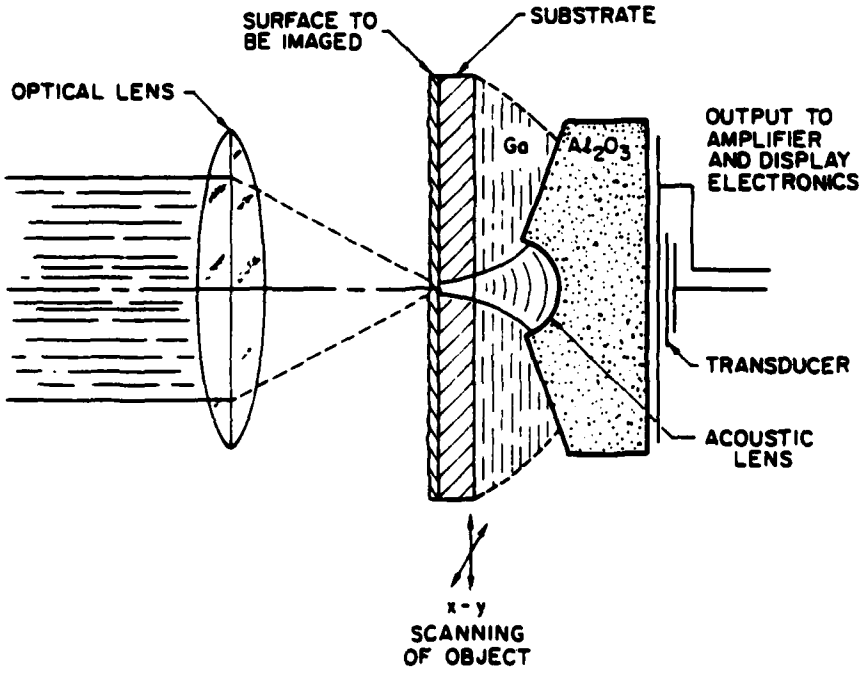

PHOTOACOUSTIC IMAGING OF A FREE SURFACE

FIGURE 3

collected through the substrate.

The new coupling scheme changes the boundary condition of the photoacoustic generation from that of a loaded surface to that of a free surface. If we were working at low frequencies, this would reduce the efficiency of photoacoustic generation by many orders of magnitude. However, because we are working at a relatively high frequency, 1 gigahertz, the difference in the conversion efficiency is small. Using a one-dimensional model we have calculated the dependence of the photoacoustic conversion efficiency on the modulation frequency. Figure 4 shows the dependence of the photoacoustic conversion efficiency on both surface loading and frequenc for a 0.5 micron silicon layer on a quartz substrate. At less than 2 GHz, the fre surface becomes as efficient as the water loaded surface.

Figure 5 shows two images taken through a 140 micron glass substrate with the gallium coupled system. The one on the left is the acoustic reflection image using gallium as the coupling liquid. Note that the resolution is poor relative to the photoacoustic image. This is due to the fact that the wavelength of the acoustics in the glass is approximately 5 microns, as compared with 1.5 microns in water. Also, there is some aberration in the acoustic path which degrades the acoustic resolution. In the photoacoustic case, however, the resolution is determined by the thermal spot size, not the acoustic collection spot size. With an optical spot size of approximately 1 micron, and a thermal diffusion length of 0.2 microns, we have a resolution of about 1.5 microns.

We have demonstrated that it is possible to image a free surface with micron resolution. This new scheme extends the class of materials that can be evaluated photoacoustically with resolution comparable to optical microscopy.

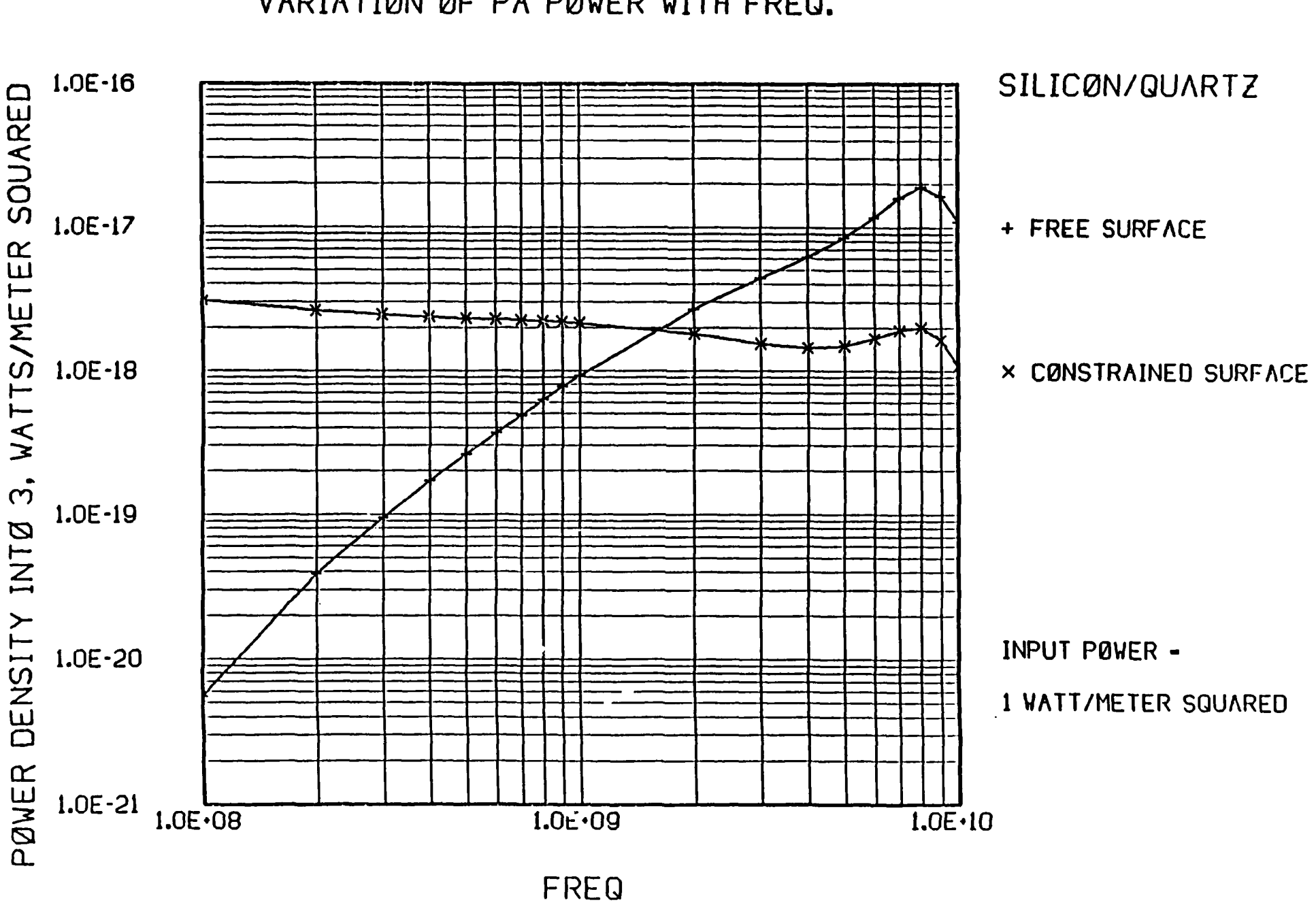
VARIATIØN ØF PA PØWER WITH FREQ.
PØWER DENSITY INTØ 3, WATTS/METER SQUARED
1.0E-16
1.0E-17
1.0E-18
1.0E-19
1.0E-20
1.0E-21
1.0E+08
1.0E+09
1.0E+10
FREQ
SILICØN/QUARTZ
+ FREE SURFACE
× CØNSTRAINED SURFACE
INPUT PØWER -
1 WATT/METER SQUARED

FIGURE 4

IMAGING THROUGH SUBSTRATE

Acoustic Reflection

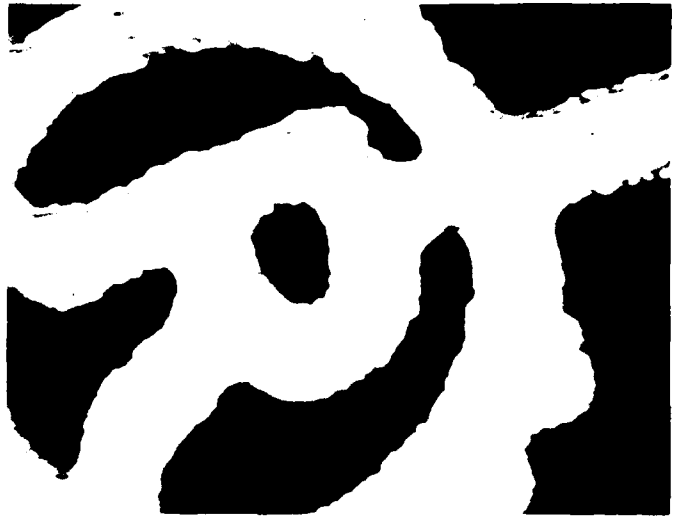

Photoacoustic

Field Size 100 micron

Frequency 1 Ghz

1000 Angs. Gold on 140 micron Glass Substrate

FIGURE 5

SECTION 4

THREE-DIMENSIONAL PHOTOACOUSTIC THEORY

4.1 Acoustic Field Equations in the Presence of Heat

We wish to derive the acoustic field equations in the presence of non-uniform heating for an isotropic solid. The stress-strain relationship for an isotropic solid is given by

$$\underline{T} = [c] \underline{S},$$

where $\underline{T}$ is the acoustic stress tensor, $[c]$ is the stiffness tensor, and $\underline{S}$ is the strain tensor[1].

The presence of non-uniform temperature produces an additional strain which does not contribute to the stress[2]. If we define:

$\underline{S_\theta}$ = strain due to non-uniform temperature

$\underline{S_a}$ = strain due to acoustic forces (no temperature)

$\underline{S} = \underline{S_\theta} + \underline{S_a}$ = total strain

Then the stress-strain relation for an isotropic solid with a non- uniform temperature distribution is given by

$$\underline{T} = [c]\underline{S_a} = [c](\underline{S} - \underline{S_\theta}) = [c]\underline{S} - [c]\underline{S_\theta}.$$

The strain due to non-uniform temperature is purely dilational. It is given by

$$\underline{S_\theta} = \alpha\theta \begin{pmatrix} 1 \\ 1 \\ 1 \\ 0 \\ 0 \\ 0 \end{pmatrix},$$

where α = linear coefficient of expansion and θ = temperature difference between actual temperature and some reference temperature of the body. Taking the

product of the isotropic stiffness tensor and the thermal strain tensor, we obtain

$$[c]\underline{S_\ell} = (c_{11} + 2c_{12})\alpha\theta \begin{pmatrix} 1 \\ 1 \\ 1 \\ 0 \\ 0 \\ 0 \end{pmatrix} = B\beta\theta \begin{pmatrix} 1 \\ 1 \\ 1 \\ 0 \\ 0 \\ 0 \end{pmatrix},$$

where B = bulk modulus and α = volume expansion coefficient. Under these conditions, therefore, the stress-strain relation is given by

$$\underline{T} = [c]\underline{S} - B\beta\theta \begin{pmatrix} 1 \\ 1 \\ 1 \\ 0 \\ 0 \\ 0 \end{pmatrix}.$$

To obtain the acoustic field equations, we take the divergence of the stress and equate it to the density-acceleration product at each point.

$$\nabla \cdot \underline{T} = \rho \frac{\partial \vec{v}}{\partial t}$$

After quite some algebra, we obtain

$$\nabla \cdot \underline{T} = (\lambda + 2\mu)\nabla(\nabla \cdot \vec{u}) - \mu(\nabla \times \nabla \times \vec{u}) - B\beta\nabla\theta.$$

Since the acoustic source is only dilational, we need not consider any displacement which is rotational, so we can set the curl of equal to zero. This also means that the gradient of the divergence of the displacement is just the Laplacian of the displacement. So the vector displacement equation becomes (for irrotational displacements)

$$(\lambda + 2\mu)\nabla^2\vec{u} = \rho\frac{\partial^2\vec{u}}{\partial t^2} + B\beta\nabla\theta.$$

We now consider the solution to this equation for a temperature source term which is spherically symmetric, i.e., it depends only on radius. This symmetry requires that all displacements must be radial, and all derivatives transverse to the radius vector must vanish. In spherical coordinates the equation becomes the scalar expression

shown below.

$$(\lambda + 2\mu)\frac{\partial}{\partial r}\left(\frac{1}{r^2}\frac{\partial}{\partial r}(r^2 u_r)\right) = \rho\frac{\partial^2}{\partial t^2}u_r + B\beta\frac{\partial\Theta}{\partial r}$$

Integrating with respect to r and differentiating with respect to time, we obtain

$$(\lambda + 2\mu)\left(\frac{1}{r^2}\frac{\partial}{\partial r}(r^2 v_r)\right) = \rho\frac{\partial^2}{\partial t^2}\int v_r dr + B\beta\frac{\partial\theta}{\partial t}.$$

If we define a velocity potential such that

$$v_r = \frac{\partial\Phi}{\partial r},$$

or equivalently,

$$\Phi = \int v_r dr + constant,$$

we obtain,

$$(\lambda + 2\mu)\nabla^2\Phi = \rho\frac{\partial^2}{\partial t^2}\Phi + B\beta\frac{\partial\theta}{\partial t} + constant.$$

The constant is indistinguishable from a uniform temperature change of the entire volume, which will not effect our a.c. excitation and solution. We can, therefore, set it to zero, leaving

$$\nabla^2\Phi - \left(\frac{1}{V_a^2}\right)\frac{\partial^2\Phi}{\partial t^2} + \left(\frac{B\beta}{\lambda + 2\mu}\right)\frac{\partial\theta}{\partial t},$$

where $V_a^2 = \frac{\lambda+2\mu}{\rho}$ and $v_r = \frac{\partial\Phi}{\partial r}$. This is the acoustic field equation then for a spherically symmetric thermal source in an isotropic elastic medium. We now must calculate the temperature distribution generated by optical power absorbed at a point.

4.2 Temperature Dis ı Point Heat Source

For an absorbed power at a point of

$$P_0 e^{j\omega t},$$

the steady state temperature distribution is[3]

$$\theta(r,\omega) = \frac{P_0}{4\pi K}\left(\frac{e^{k_t r}}{r}\right)e^{j\omega t}.$$

4.3 Solution

Using the temperature distribution above as the source term in the acoustic field equation, we obtain

$$\nabla^2\Phi + k_a{}^2\Phi = \gamma\frac{e^{-jk_t r}}{r},$$

where

$$\gamma = \left(\frac{B\beta}{\lambda + 2\mu}\right)\left(\frac{j\omega P_0}{4\pi K}\right).$$

The general solution to this equation is given by

$$\Phi = \frac{ae^{-jk_a r}}{r} + \left(\frac{\gamma}{k_t{}^2 + k_a{}^2}\right)\frac{e^{-k_t r}}{r}.$$

To determine the coefficient a , we must impose the boundary condition that the radial velocity must go to zero at the r = 0. This means that the gradient of the potential function must be zero at the origin. Under these conditions, the total solution is

$$\Phi = \frac{-\gamma}{k_t{}^2 + k_a{}^2}\left(\frac{e^{-jk_a r}}{r} - \frac{e^{-k_t r}}{r}\right).$$

To examine the efficiency of photoacoustic conversion, we calculate the acoustic power radiated from the source. Since the power radiated is independent of r , we calculate the Poynting vector far from the source since there the wave becomes a plane wave, and, therefore, we can use the plane wave impedance to calculate the Poynting vector. Far from the source, the velocity is given by

$$v_r \approx \left(\frac{jk_a\gamma}{k_t{}^2 + k_a{}^2}\right)\left(\frac{e^{-jk_a r}}{r}\right).$$

The impedance is

$$Z_0 = \frac{-T_r}{v_r} = -\rho V_a.$$

The total power radiated is, therefore

$$P = 2\pi(\rho V_a)\left(\frac{B\beta}{\lambda + 2\mu}\right)^2\left(\frac{P_0}{4\pi K}\right)^2 \frac{\omega^2 {k_a}^2}{|k_t|^4 + {k_a}^4}.$$

In another form,

$$P = 2\pi(\rho V_a)\left(\frac{B\beta}{\lambda + 2\mu}\right)^2\left(\frac{P_0}{4\pi K}\right)^2 \frac{\kappa^2 {k_a}^2}{\left(1 + \frac{\omega^2\kappa^2}{{V_a}^4}\right)}.$$

4.4 Discussion

We now consider the frequency dependence of the photoacoustic conversion efficiency. At low frequencies,

$$\frac{\omega^2\kappa^2}{{V_a}^4} \ll 1$$

so the acoustic power generated for a given absorbed optical power is

$$P = 2\pi\left(\frac{\rho}{V_a}\right)\left(\frac{B\beta}{\lambda + 2\mu}\right)^2\left(\frac{P_0}{4\pi}\right)^2\left(\frac{1}{\rho C}\right)^2\omega^2$$

Note that the radiated power is proportional to the square of the modulation frequency. This result is for the case of a modulated point source of heat in an infinite volume with no boundaries. If we consider the effect of positioning the source near the surface of an infinite half space, we find that the free surface increases the dependence on the frequency of the modulation for the following reason. In the low frequency regime, which is somewhere below 100 GHz, the ratio of thermal source size to acoustic wavelength is small, but increases with frequency. The coupling from the thermal distribution to the acoustic wave in the presence of a free surface increases with frequency due to the fact that the reflections from the free surface are out of phase with forward traveling waves, and they tend to cancel.

At low frequencies, they cancel almost exactly, whereas at higher frequencies, the cancellation is smaller. Thus, the overall coupling increases with frequency in the presence of the free surface. This means that the intensity in the far field goes as

$$I \sim \omega^N$$

where $N > 2$ when the thermal source is near a free surface. An exact calculation of this dependence on frequency is presently being done.

We now compare these results to those obtained using a one- dimensional model. R. M. White treated this problem[4]. The first case we consider is where the absorption of optical power takes place in an infinitesimally thin boundary plane between two semi- infinite half spaces acoustically bonded together. The acoustic power density for this case is given by

$$I_a = \frac{1}{8}\left(\frac{V_a}{\rho}\right)\left(\frac{B}{c_{11}}\right)^2\left(\frac{\alpha}{C}\right)^2 P_0^2$$

Note that the generated acoustic power density is independent of the modulation frequency in this low frequency limit. Recalling our earlier result, we find that for the case of a point source of modulated heat in an infinite plane, the generated acoustic power depended on the square of the modulation frequency. This indicates that for highly focused optical sources, the modulation frequency should be as high as possible. for maximum conversion efficiency. In the plane wave case, the conversion efficiency is independent of frequency.

We also consider and compare the one-dimensional case with the three- dimensional case when the source is near a free surface. From White, we find that the acoustic power density generated by an infinitesimal boundary absorption at the free surface is

$$I_a = \frac{1}{2Z_0}\left(\frac{K}{\rho C}\right)\left(\frac{B}{c_{11}}\right)^2\left(\frac{\alpha}{C}\right)^2 P_0^2 \omega$$

Due to the effects of coupling, the one-dimensional conversion efficiency at a free surface depends on the first power of the frequency. However, in the case of a point source near a free surface, the conversion efficiency depends on the modulation frequency by some power greater than two.

It is clear that the modulation frequency should be as high as is possible when the thermal source size is small compared to an acoustic wavelength for optimal conversion efficiency. One-dimensional theory does not predict this in the constrained case, and predicts only an increase proportional to the frequency in the free surface case. We are presently using a diffraction limited optical spot size for maximum resolution in our images. This is the reason for working at 1 GHz modulation frequencies. The frequency could still be increased by more than 100 and still be in the low frequency limit. When imaging materials with strong optical absorption, increasing the modulation frequency could result in substantial improvements in the sensitivity of the imaging system.

SECTION 5

IMAGING WITH A DIODE LASER AS THE OPTICAL SOURCE

We have recently imaged photoacoustically with micron resolution using a 5 milliwatt diode laser as the optical source. This demonstration is an indication of the tremendous sensitivity that we have because of the fact that we have an acoustic lens rather than a flat piezoelectric transducer. This demonstration gives us an experimental verification of this sensitivity, as well as a calibration for the system for use in considering what other experiments may be possible. The use of the diode decreases the cost of the optical source from over twenty thousand dollars to less than five hundred dollars. The diode was modulated at 1 gigahertz directly with a biased rf source, eliminating the need for any external electro-optic modulator and all the problems associated with modulators at high frequencies.

Decreasing the input power from 100 milliwatts to 5 milliwatts is a significant jump due to the fact that the generated acoustic power is proportional to the square of the input optical power. Therefore, we expected a decrease in signal power by more than 25 db. To increase our sensitivity, we used a heterodyne detection scheme which allowed us to reduce the bandwidth of the signal by running cw . With a narrow band signal, we were able to reduce the noise in the system by almost 30 db, enough to compensate for the loss in the signal. In Figure 6 is found an 'a-trace' demonstrating the signal to noise achieved with this system.

Figure 6:

This experiment has given us a good experimental value for the sensitivity of our imaging system for use in determining what future experiments may be possible. These experiments follow in the next section.

SECTION 6

HIGH RESOLUTION ACOUSTO-OPTIC LASER PROBE

6.1 Introduction

There have been several high resolution acoustic probes reported in the literature over the last several years. Interferometry, beam deflection, and acoustic lenses have been used to measure photoacoustic and acoustic field distributions[5–10]. We now present a new acousto-optic probe which exploits the photoelastic coupling between optical and acoustical fields in a high pressure gas under collinear Bragg scattering conditions. This probe was designed to detect sound generated photothermally at the surface of a solid; however, sound transmitted through an object into the high density gas can also be measured with good sensitivity. The probe has several features which look attractive. It is a non-contacting, all optical technique which requires no acoustic transduction. Its operating frequency is near 1 GHz, constrained there by the collinear Bragg resonance. The resolution of the probe is determined by the optical spot size, which can be submicron.

6.2 Theory

Bragg Reflectivity

When sound propagates through a high density gas, the fluctuations in the local density cause a perturbation of the index of refraction. This perturbation of the dielectric constant causes a scattering of light which is incident upon the perturbed gas. Under proper phase matching conditions, i.e. the Bragg condition, the scattering can be significant. To calculate the efficiency of this interaction between the sound and incident light, we must first derive the photoelastic constant, which relates the condensation of the gas to the perturbation of the dielectric

constant. We can derive the photoelastic constant for an ideal gas using the Lorentz-Lorenz formula[11].

$$\alpha_{pol} = \frac{3\epsilon_0(\epsilon - 1)}{N(\epsilon + 2)} \tag{1}$$

where α_{pol} is the mean polarizability of the atoms or molecules, ϵ_0 is the permittivity of free space, ϵ is the relative dielectric constant,and N is the number of atoms or molecules per unit volume. For a gas, where $(\epsilon - 1)$ is much less than 1, it can be shown that

$$(\epsilon - 1) \approx \frac{N\alpha_{pol}}{MW\epsilon_0}\rho \tag{2}$$

where MW is the molecular or atomic weight of the medium, and ρ is the density. Taking the derivative of equation 2, we find that for a small change in density $\delta\rho$, the corresponding change in the relative dielectric constant $\delta\epsilon$ is given by

$$\delta\epsilon = (\epsilon - 1)\frac{\delta\rho}{\rho_0} = (\epsilon - 1)S \tag{3}$$

where $S=(\rho-\rho_0)/\rho_0$ is the acoustic condensation. When light propagates through the gas simultaneously with the sound, a nonlinear polarization wave is generated whose amplitude is proportional to the product of the acoustic and electromagnetic fields. This polarization wave radiates optical power at the sum and difference frequencies of the acoustic and optical waves. When the wavelength of the sound in the gas is one half that of the light, phase matching takes place for collinear propagation of the light and the sound. The incident light is back reflected from the sound wave. See Figure 7.

The efficiency of the scattering can be called a 'Reflectivity'. Using Maxwell's equations to obtain the inhomogeneous wave equation, and the photoelastic relation, we can calculate the power reflectivity Γ due to the sound wave in the gas. The result for the k vector matched case is given by

$$\Gamma = \left[\frac{\pi(\epsilon - 1)S_0}{2\alpha\lambda_0}\right]^2 \tag{4}$$

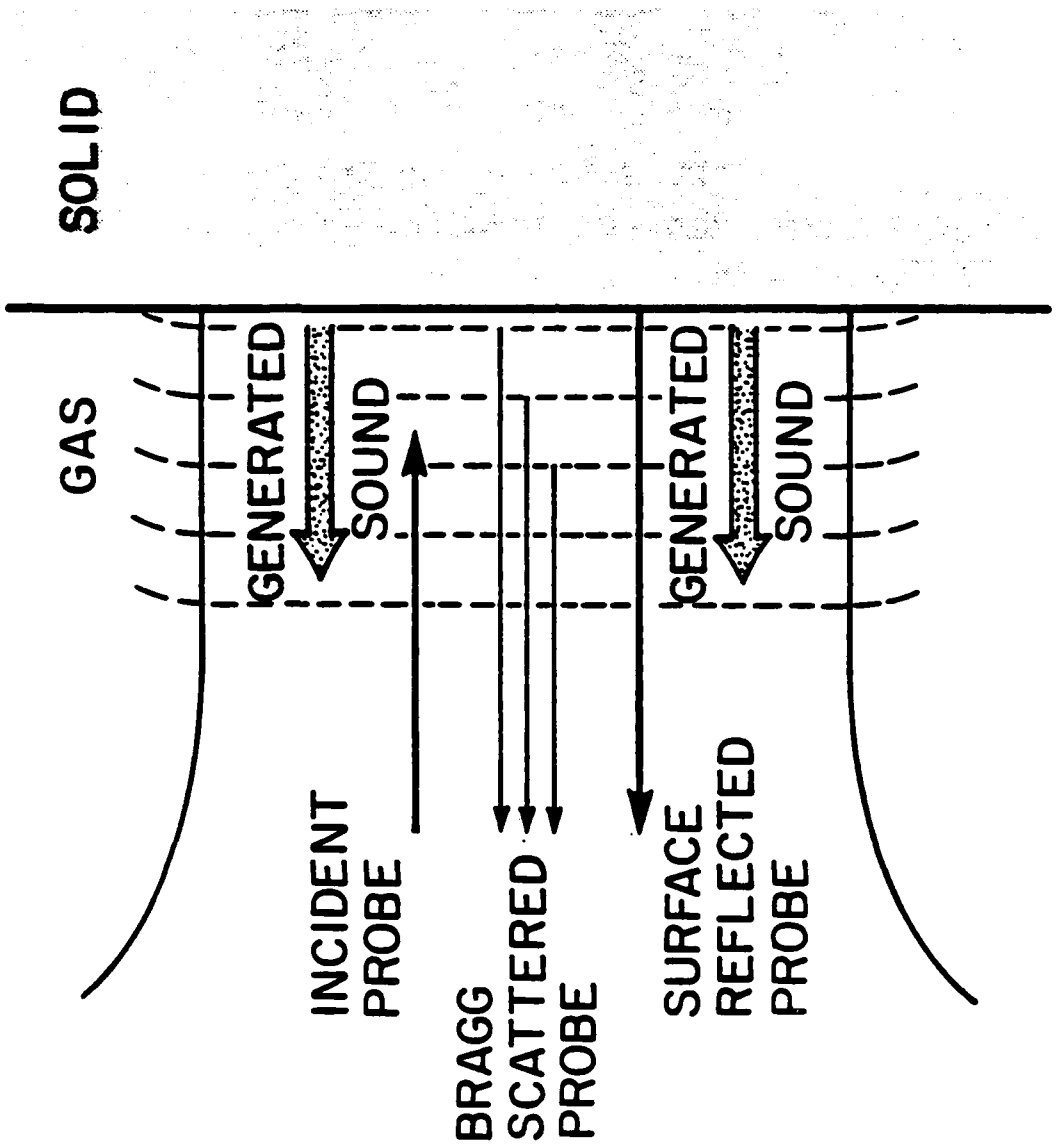
SOLID
GAS
GENERATED SOUND
GENERATED SOUND
INCIDENT PROBE
BRAGG SCATTERED PROBE
SURFACE REFLECTED PROBE

FIGURE 7

where ϵ is the relative dielectric constant of the gas, S_0 is the peak condensation in the gas, α is the attenuation constant of the gas, and λ_0 is the wavelength of the incident light in the gas.

Frequency Dependence

As mentioned in the previous section, the Bragg interaction depends on k-vector matching of the incoming and reflected light fields with the acoustic field. It can be shown that the magnitude of the Bragg scattered field depends on the k-vector mismatch Δk according to

$$\left|\sqrt{\Gamma}\right| \sim \left|\int_0^\infty e^{-\alpha z} e^{j\Delta k z} dz\right| = \left|\frac{1}{\sqrt{\alpha^2 + \Delta k^2}}\right|. \tag{5}$$

The signal is proportional to the power reflectivity, therefore

$$P_{signal} \sim \Gamma = \left[\frac{\pi(\epsilon - 1)S_0}{2\lambda_0}\right]^2 \left(\frac{1}{\alpha^2 + \Delta k^2}\right) \tag{6}$$

where $\Delta k = k_0 - k_a + k_e \approx 2k_0 - k_a$. In terms of frequency, $\Delta k = (w - w_0)/V_a$, where w_0 is the acoustic frequency at which Δk is zero, and V_a is the velocity of sound in the gas. As can be seen from equation 5, there is a Fourier transform relationship between the spatial dependence of the acoustic wave and the frequency dependence of the Bragg interaction. Because the acoustic wave is exponentially damped, the frequency dependence is Lorentzian. The theoretically expected frequency dependence, with some experimental data taken, is shown in Figure 8.

Pressure Dependence

The efficiency of the Bragg scattering depends upon the pressure of the gas through the dielectric constant and the acoustic attenuation constant. These parameters of the gas depend upon the pressure in the following way.

$$(\epsilon - 1) \sim \rho \sim P_{gas} \tag{7}$$

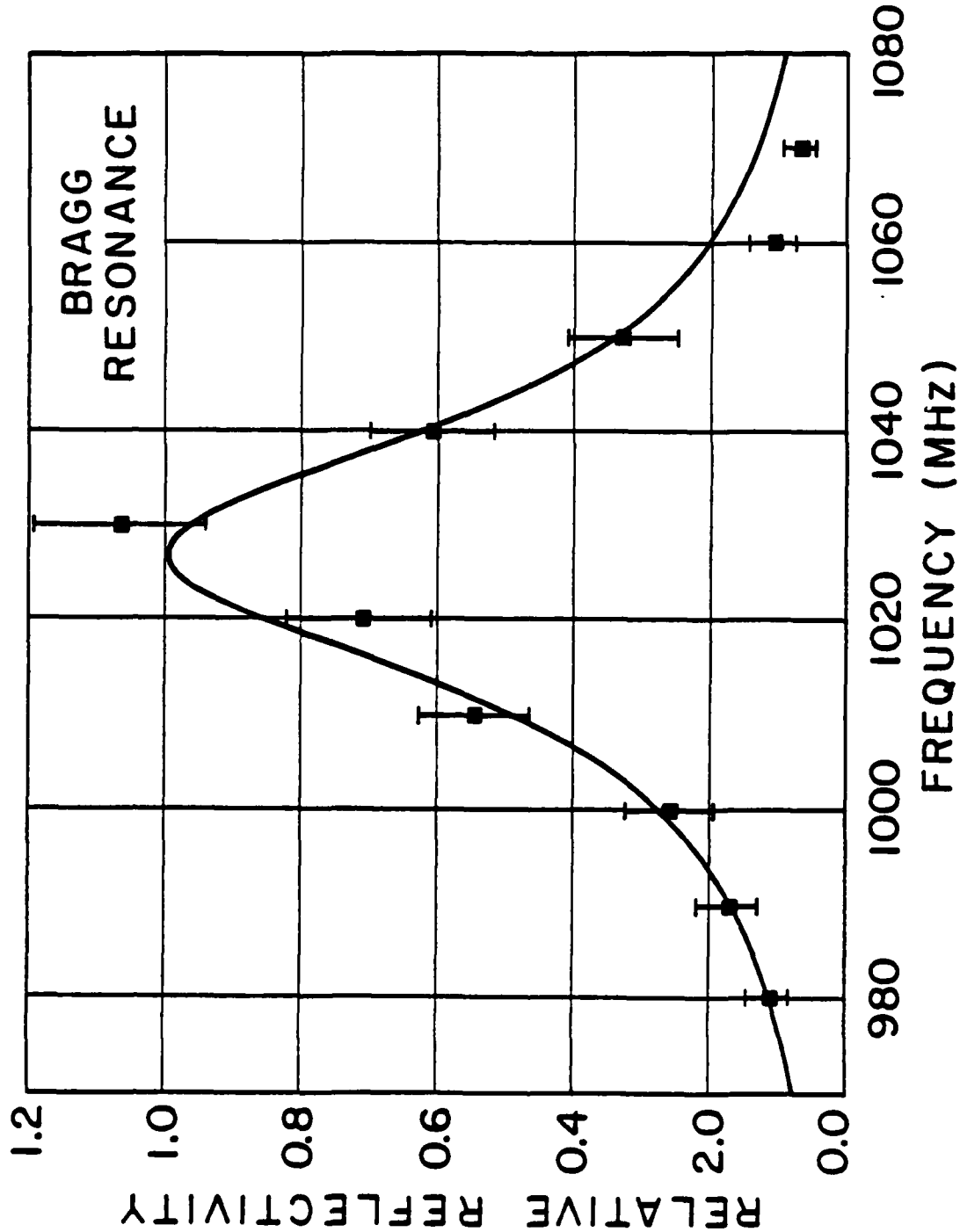
BRAGG
RESONANCE
RELATIVE REFLECTIVITY
1.2
1.0
0.8
0.6
0.4
2.0
0.0
980
1000
1020
1040
1060
1080
FREQUENCY (MHz)

FIGURE 8

$$\alpha \sim \frac{1}{P_{gas}} \tag{8}$$

Substituting equations 7 and 8 into equation 4, we find that

$$\Gamma \sim P_{gas}{}^4 S_0^2. \tag{9}$$

If we relate the reflectivity to the acoustic power density in the gas, we find that

$$S_0^2 = \frac{2I_a}{\rho V_a^3}, \tag{10}$$

where

$$\rho \sim P_{gas}. \tag{11}$$

and

$$V_a \sim constant \tag{12}$$

Therefore, Γ goes as the third power of the pressure of the gas for a given acoustic intensity.

$$\Gamma \sim P_{gas}{}^3 I_a \tag{13}$$

Heterodyne Detection

We will now look at the sensitivity of this probe to acoustic power either photothermally generated, or transmitted from a solid to the gas. The incident probe beam of average power P_0 is reflected by the sound in the gas with power reflection coefficient Γ, and reflected from the sample surface with power reflection coefficient R. Both reflected components propagate collinearly back to the photodetector where they generate a heterodyne signal at the frequency of the acoustic wave in the gas. The optical heterodyne power is proportional to the product of the fields from these two reflections. The peak optical heterodyne power at frequency (w_a) is given by

$$P_{het} = 2\sqrt{RP_0}\sqrt{\Gamma P_0} = 2\sqrt{R}\sqrt{\Gamma}P_0. \tag{14}$$

Conversion of the optical heterodyne power to an RF signal takes place in the photodetector. The peak heterodyne current is given by

$$I_{het} = \alpha_r P_{het}, \tag{15}$$

where α_r is the responsivity (amps/watt) of the photodetector. The average signal power into the load resistor is thus given by

$$P_{signal} = \frac{1}{2} I_{het}^2 R_l = 2\alpha_r{}^2 R\Gamma P_0{}^2 R_l. \tag{16}$$

There are three sources which contribute noise to the signal as it is detected and amplified. They are shot noise, Johnson noise, and amplifier noise. The total noise power contributed by these three sources is given by[5,6]

$$P_{noise} = 4KTBF + 2e\alpha_r BRP_0 R_l, \tag{17}$$

where K is the Boltzman's constant, T is the absolute temperature, B is the bandwidth, F is the noise figure of the preamplifier, e is the electron charge, α_r is the detector responsivity(A/W), R_l is the load resistance, and P_0 is the average detected power. Thus the signal-to-noise ratio is given by

$$\frac{S}{N} = \frac{2\alpha_r{}^2 R\Gamma P_0{}^2 R_l}{4KTBF + 2e\alpha_r BRP_0 R_l}. \tag{18}$$

Sensitivity to Bragg Reflectivity

Rearranging equation 18, we can calculate the minimum reflectivity measurable for a given signal-to-noise ratio.

$$\Gamma = \left(\frac{S}{N}\right) \frac{(4KTBF + 2e\alpha_r BRP_0 R_l)}{2\alpha_r{}^2 RP_0{}^2 R_l} \tag{19}$$

Under the following conditions,

B = 5 Hz (.1 sec integration time)

F = 1.77 (2.5 db noise figure of preamplifier)

α_r = .33 a/w (detector responsivity)

P_0 = 1.0 mW (incident optical power)

R = 1 (sample reflectance)

R_l = 50 Ω (load resistance)

the minimum reflectivity detectable with a given signal-to-noise is

$$\Gamma = \left(\frac{S}{N}\right)(1.5 \times 10^{-14}). \tag{20}$$

Therefore, a Bragg reflectivity of approximately 10^{-14} should be detectable with a signal-to-noise of one.

Sensitivity to Acoustic Power

We can now relate the Bragg reflectivity to the acoustic power density to determine the sensitivity to acoustic power. Using equations 4 and 11, we obtain an expression for the reflectivity Γ in terms of the acoustic intensity I_a.

$$\Gamma = \left[\frac{\pi(\epsilon - 1)}{2\alpha\lambda_0}\right]^2\left(\frac{2I_a}{\rho V_a{}^3}\right) \tag{21}$$

Using values for argon gas at 100 atmospheres[12,13],

$(\epsilon - 1) = .055$

$V_a \approx 323$ m/s

$\rho = 160$ kg/m^3

$\alpha = 1.7 \times 10^5 m^{-1}$

$\lambda_0 = .6328 \times 10^{-6} m$

the reflectivity is calculated in terms of the acoustic intensity.

$$\Gamma = (2.1 \times 10^{-10})I_a \tag{22}$$

Using the results from equations 20 and 22, we can now calculate the minimum acoustic intensity measurable for a given signal-to-noise ratio.

$$I_a = (7.4 \times 10^{-5})(S/N) \tag{23}$$

For a signal-to-noise ratio of one, we should be able to detect less than $10^{-4} W/m^2$ of acoustic power over an area of approximately 1 square micron. In this case, the total detected power is less than 10^{-16} watts. The corresponding surface displacement under these conditions is less than 10^{-4} angstroms.

6.3 Experimental Arrangement

A schematic diagram of the acousto-optic probe set up is shown in Fig. 9. This is the arrangement used for detecting photothermally generated sound. A modulated pump laser is focused by an optical microscope objective inside the gas cell to a diffraction limited spot on the sample surface. The probe laser is also focused at the same location. The modulated pump laser photothermally generates sound which propagates into the sample as well as into the gas. The amount of sound generated depends upon the properties of the sample. The probe laser is reflected at the sample surface with no shift in frequency, as well as reflected and frequency shifted by the sound wave propagating in the gas. The quarter wave plate outside the cell allows the reflected light to be transmitted through the polarizing beamsplitter, and is focused onto a fast photodetector. The photodetector is isolated from the pump laser by a narrowband spike filter placed in front of the detector. The sample is positioned for focus and translated by two micrometers from outside the gas cell. A reference signal at the frequency of the axial mode spacing of the probe laser (w_r) is detected in a second photodetector.

To avoid the problems of RF interference that occur when detecting at the modulation frequency of the pump laser (w_a), the two longitudinal modes of the

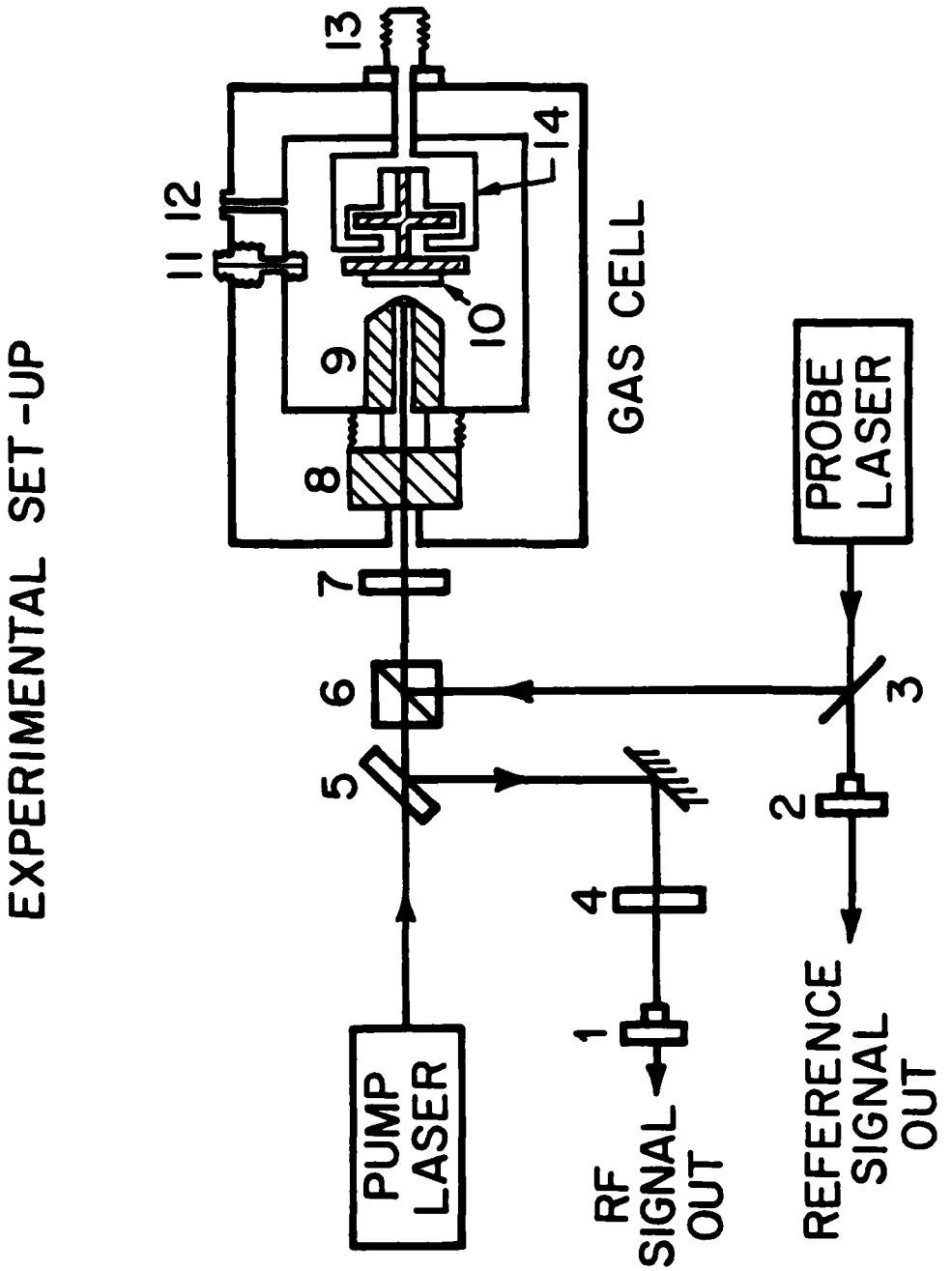
EXPERIMENTAL SET-UP
PUMP LASER
PROBE LASER
RF SIGNAL OUT
REFERENCE SIGNAL OUT
GAS CELL
1
2
3
4
5
6
7
8
9
10
11
12
13
14

FIGURE 9

He-Ne probe laser are used to mix the heterodyne signal to a frequency other than that of the acoustic wave. This is accomplished by optically mixing the Bragg shifted signal from one axial mode ($w_o + w_a$) with the unshifted frequency of the second axial mode ($w_o + w_r$). The result is a heterodyne signal at the difference between the acoustic frequency and the axial mode spacing ($w_a - w_r$). Electronically mixing the reference signal (w_r) with the master oscillator (w_a) and adding a 10.7 MHz local oscillator generates an RF signal at ($w_a - w_r + 10.7$ MHz) which can then be used to mix the optical signal down to 10.7 MHz. It is then passed through a crystal filter with a 10 kHz bandwidth. The detection scheme can be seen in figure 10.

6.4 Experimental Results

Frequency dependence

The frequency dependence of the Bragg interaction was measured in the following way. A sapphire flat with a 1 GHz acoustic transducer on one side, and an amorphous carbon matching layer on the other was placed in the gas cell. It was positioned so that the incident light was focused onto the carbon layer where the acoustic power was incident from the sapphire. RF pulses were then sent to the transducer, generating acoustic power which propagated down the sapphire flat into the gas. The acoustic power in the gas then generated an acousto-optic signal which was measured. The frequency of the RF input was varied, and at each frequency, the insertion loss of the transducer was measured using a pulsed reflection technique. Also, the transmission factor from sapphire to the gas was calculated including the effects of the carbon matching layer. The measurement of the acousto-optic signal, made at each frequency, was then normalized by the proper transmission factor and insertion loss for that frequency. The experimental results are shown with the

DETECTION ELECTRONICS

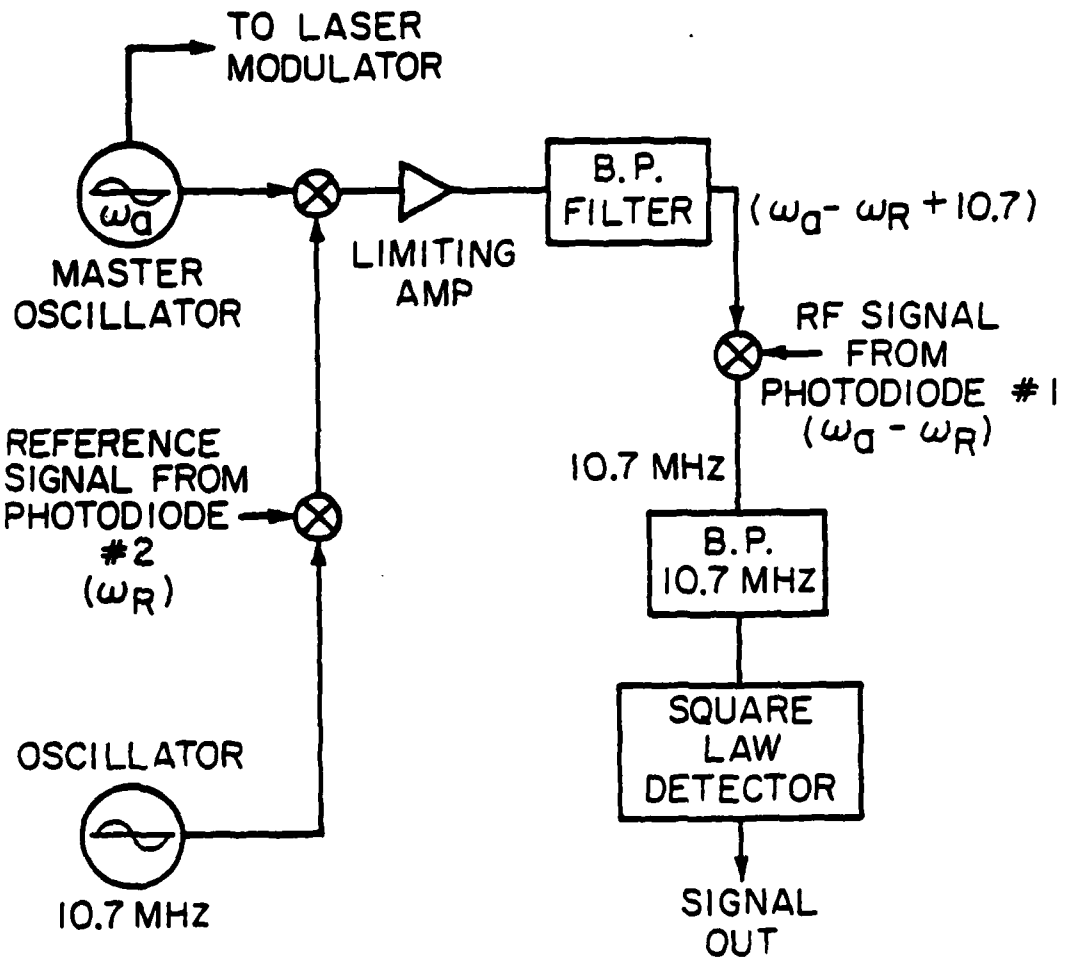

FIGURE 10

theoretical frequency dependence in Figure 8. There is good agreement between theory and experiment.

Absolute Sensitivity

A measurement of the absolute sensitivity of the probe at 50 atmospheres was made using the acoustic flat mentioned above. In this experiment, the peak power of the input RF pulses, along with the insertion loss, was measured at the Bragg resonance frequency. This information allowed a determination of the total acoustic power in the sapphire flat. The acoustic spot size at the carbon matching layer was calculated numerically. Also, the transmission from the flat to the gas was calculated taking into account the effects of the matching layer. This information made possible the calcuation of the absolute acoustic power density in the gas.

A measurement of the acousto-optic signal-to-noise ratio was then measured, along with the incident and detected optical power levels. Below are found the experimental and calculated data.

$P_{gas} = 50$ atmospheres

$P_0 = 1.75mW$

$R_{eff} = .04$

F = 1.77

B= 5 MHz

$R_l = 50\Omega$

Using these values,the theory predicts that the minimum acoustic intensity detectable with a signal-to-noise of one is

$$I_{a_{min}} = 3.9 \times 10^3 W/m^2. \tag{24}$$

The measured minimum detectable acoustic intensity was

$$I_{a_{min}} = 5.5 \times 10^4 W/m^2. \tag{25}$$

This means that experimental results deviate from that predicted by theory by a factor of 14.1 in acoustic power.

One of the sources of the discrepancy between the predictions from the theory and the experimental measurement is that the probe laser used in this experiment has two axial modes which are used to allow detection at a frequency other than the acoustic frequency. The theory assumed a single mode laser probe. Using a two mode probe laser reduces the expected sensitivity to acoustic power by a factor of 4. This leaves a discrepancy of a factor of 3.5. The source of this factor is presently uncertain.

Note that under these experimental conditions, the detection is Johnson noise limited. By using a probe laser modulated near the acoustic frequency, detection of the heterodyne power could be done at low frequencies, allowing for a large load resistance. The detection would then become shot noise limited. In this case, the sensitivity to acoustic power would increase by more than a factor of 30.

Pressure Dependence

The dependence of the signal on pressure was measured in the following way. The signal power was measured while varying the gas pressure in the cell for constant input RF power. Since the transmission of acoustic power from the sapphire to the gas varies with gas pressure (the impedance of the gas is proportional to it's density), the signal was normalized by this transmission factor. The measured pressure dependence was

$$P_{signal} \sim {P_{gas}}^{2.5} \tag{26}$$

over a pressure range of 26 to 66 atmospheres. The theory predicts that it should go as the third power of the gas pressure.

6.5 Applications

The primary application for this probe is to detect photoacoustically generated sound near 1 GHz. The reasons for this are the following. Although the sensitivity of this probe is comparable to displacement interferometry for detection of acoustic power transmitted through an object, its sensitivity to photoacoustically generated acoustic power at the surface of a solid is more than an order of magnitude greater than that of photodisplacement at frequencies near 1 GHz. This is due to the fact that the acoustic power thermally generated in the gas is much greater than the thermally generated power coupled from the solid to the gas via surface displacement. The second reason is that one dimensional theory predicts an inverse dependence upon the thermal conductivity for strongly absorbing solids. This means it may be possible to measure and spatially map thermal conductivities with high resolution. At frequencies near 1 GHz, the thermal wavelength in most solids is less than 1000 angstroms. The photothermal resolution would essentially be determined by the optical spot size. Some interesting candidates for study may be silicon and gallium arsenide devices which have been implanted or doped to modify their electrical conductivity with high spatial definition. The capability to measure the thermal conductivity on a microscopic scale may prove useful as a diagnostic tool in the processing of integrated circuits.

REFERENCES

[1] B. A. Auld, *Acoustic Fields and Waves in Solids*, Volume 1, New York: John Wiley &Sons, 1973, p. 27.

[2] A. E. Love, *The Mathematical Theory of Elasticity*, Cambridge: Cambridge University Press, 1927 (Dover reprint, 1944), 4th ed., p. 108.

[3] H. S. Carslaw and J. C. Jaeger, *Conduction of Heat in Solids*, London: Oxford University Press, 1959, 2nd ed., p. 263.

[4] R. M. White, "Generation of elastic waves by Transient Surface Heating," J. Appl. Phys. 34, 3559 (1963).

[5] R. L. Whitman and A. Korpel, "Probing of Acoustic Surface Perturbations by Coherent Light," Appl. Opt. 8, 1567 (1969).

[6] R. M. De La Rue, R. F. Humphryes, I. M. Mason, and E. A. Ash, "Acoustic-surface-wave amplitude and phase measurements using laser probes," Proc. IEE 119, 117 (1972)

[7] R. L. Jungerman, J. E. Bowers, J. B. Green, and G. S. Kino, "Fiber Optic Laser Probe for Acoustic Wave Measurements," Appl. Phys. Lett. 40, 313 (1982)

[8] J. E. Bowers, "Fiber-Optic Sensor for Surface Acoustic Waves," Appl. Phys. Lett. 41, 231 (1982)

[9] H. K. Wickramasinghe, R. Bray, V. Jipson, C. Quate and J. R. Salcedo, "Photoacoustics on a Microscopic Scale," Appl. Phys. Lett. 1978, Vol. 33, p. 923

[10] S. Ameri, E. A. Ash, V. Neuman, C. R. Petts, "Photo-displacement Imaging", Electr. Lett. 17, p.337 (1981)

[11] M. Born and E. Wolf, *Principles of Optics*, Sixth Ed., p. 87, Pergamon Press (1980)

[12] H. K. Wickramasinghe and C. R. Petts, "Gas Medium Acoustic Microscopy," *Scanned Image Microscopy*, p. 59, Academic Press (1980)

[13] Gerard A. Cook, *Argon, Helium, and the Rare Gases The Elements of the Helium Group*, p.240, Interscience Publishers, New York (1961)

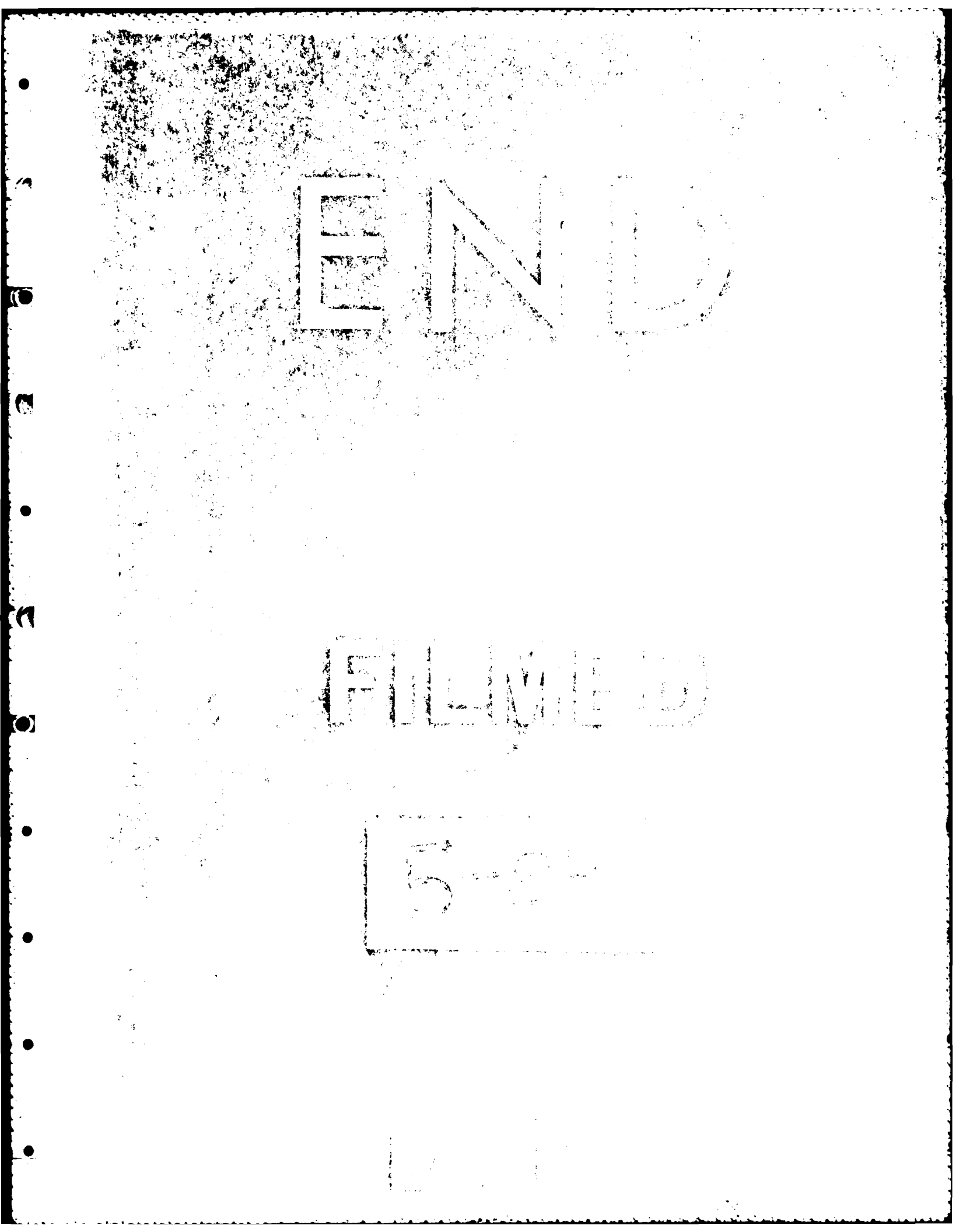
END
FILMED